Exploring Cognitive States: Methods for Detecting Physiological Temporal Fingerprints

Nicholas J. Napoli[1], *MuditPaliwal*[6]
Industrial and Systems Engineering, University of Florida, Gainesville, FL, 32611, USA

Stephen Adams[2], *WilliamT.Scherer*[7]
Systems and Information Engineering, University of Virginia, Charlottesville, VA, 22903, USA

Angela Harrivel[3], *KellieD.Kennedy*[5], *ChadL.Stephens*[4]
NASA Langley Research Center, Hampton, VA 23681

Cognitive state detection and its relationship to observable physiologically telemetry has been utilized for many human-machine and human-cybernetic applications. This paper aims at understanding and addressing if there are unique psychophysiological patterns over time, a "physiological temporal fingerprint", that is associated with specific cognitive states. This preliminary work involves commercial airline pilots completing experimental benchmark task inductions of three cognitive states: 1) Channelized Attention (CA); 2) High Workload (HW); and 3) Low Workload (LW). We approach this objective by modeling these "fingerprints" through the use of Hidden Markov Models and Entropy analysis to evaluate if the transitions over time are complex or rhythmic/predictable by nature. Our results indicate that cognitive states do have unique complexity of physiological sequences that are statistically different from other cognitive states. More specifically, CA has a significantly higher temporal psychophysiological complexity than HW and LW in EEG and ECG telemetry signals. With regards to respiration telemetry, CA has a lower temporal psychophysiological complexity than HW and LW. Through our preliminary work, addressing this unique underpinning can inform whether these underlying dynamics can be utilized to understand how humans transition between cognitive states and for improved detection of cognitive states.

I. Introduction

This study seeks to gain an understanding of the underlying physiological sub-states associated with cognitive states (the physiological temporal fingerprint of a cognitive state) using multi-modal physiological sensing and statistical models well-suited for time-dependent data. These temporal sub-states can be thought of as distributions of psychophysiological discriminators, or specific regions within the feature space, as a given cognitive state occurs over time. The ability to understand these underlying regions within the feature space of cognitive states can improve training for vehicle operators and pilots [1, 2] and feedback systems for simulators involving human subjects [3]. Further understanding the underlying physiological temporal fingerprint of a cognitive state, can increase the understanding of what physiological systems within the human body are associated with these cognitive states and how humans transition from one cognitive state to the next. This can help drive research for improving the predictability of these states and alleviating undesired cognitive states through mitigations and countermeasures.

Prior Work: Cognitive states are not directly measurable, but can be inferred through physiological and behavioral data from the subject such as eye movement, electroencephalogram, electrocardiogram, heart rate, galvanic skin response, respiration rate, and other directly measurable modalities [4–15]. The majority of the current work within cognitive state prediction focuses on a fixed set of modalities (e.g., one or more modalities such as EEG and ECG). However within the community we have not fully characterized how different combinations of modalities affect overall predictive accuracy or how different modalities provide the necessary information to distinguish specific types of cognitive states. As such, current work focuses on prediction of cognitive state from these modalities, but does not seek an understanding of the associated physiological signatures of these cognitive states.

While there is much research in the time-dependent nature of physiological data, there is little work which focuses on the relation of this time-dependent physiological data to a corresponding cognitive state. The work which includes the time-dependent aspect of cognitive studies does not contain a thorough analysis of how multiple modalities can affect the

overall understanding of sub-state transitions and their underlying physiological distributions within the feature space. In addition, the work which does take into account the time-dependent nature of the data does so in a way which seeks only to predict cognitive states but not to understand the underlying dynamics of the physiological states [3, 16, 17].

Challenges: Research to date has focused on experimental designs which incorporate singular physiological modalities or machine learning methodologies which do not take advantage of the time-dependent nature of the data. Of the research which has incorporated multi-modal physiological sensing and machine learning methodologies which do incorporate the time-dependent nature of the data, the emphasis of analysis was on prediction of cognitive state instead of a deeper understanding of the physiological fingerprints associated with those cognitive states [18]. Modeling has focused on cognitive state as the first-order latent state instead of an underlying physiological state whose transitions could dictate a second-order latent state attributable to the current cognitive state. Therefore, this raised three questions when evaluating underlying sub-state physiological dynamics of cognitive states: 1) What physiological features should be examined for evaluating underlying sub-state physiological dynamics of cognitive states; 2) Does modeling these temporal dynamics help improve the predictive nature of cognitive state modeling; 3) Do sub-state physiological dynamics of cognitive states have a unique underlying fingerprint when compared to other cognitive states?

Insights: Hidden Markov models (HMMs) are one highly utilized machine learning method that fuses data and examines temporal transition of data. HMMs are known for their ability to infer latent states through observable emissions [19, 20]. These models have been recently used for cognitive state detection, where the cognitive states in question are the latent states and the physiological data are the observable emissions [3, 16, 17]. However, there are numerous typologies and evaluation methods of HMM from speech recognition to molecular biology [19–21]. The HMM method proposed by Duda [22], "the learning and evaluation process", builds an HMM model for each proposed cognitive state and predicts the "true" cognitive state using maximum likelihood. By leveraging this HMM design (a specific HMM is trained for each cognitive state) and equating the hidden state of the HMM to psychophysiological sub-states, we can address sub-state changes by evaluating how the HMM model transitions overtime. The transition of the underlying psychophysiological dynamics of the cognitive states (i.e., the temporal fingerprint) can be estimated using an HMM decoding algorithm, generating the discrete sequence of psychophysiological dynamics. We can then evaluate if the psychophysiological dynamics are repetitive/predictive or random/chaotic through a proposed complexity analysis called permutation entropy [4]. Through our insight of utilizing hidden Markov analysis, we hypothesis that we will be able to demonstrate that the underlying psychophysiological temporal fingerprint has a statistically unique complexity of underlying dynamics for each proposed cognitive state.

II. Methods

A. Experimental Design and Data Collection:

Twenty-one (21) commercial aviation pilots were asked to perform benchmark tasks while wearing physiological sensors which were intended to establish ground truths for cognitive state testing. The cognitive states of interest for this analysis include Channelized Attention (CA), Low Workload (LW), and High Workload (HW). These benchmark tasks include Tetris for channelized attention, and MATB (Multi-Attribute Task Battery: available at http://matb.larc.nasa.gov/) for high and low workload tasks for the high and low workload cognitive states. These benchmark tasks have been discussed previously [23]. Each task was used to induce cognitive states under controlled conditions for six minutes each and were given with the full knowledge of the participant, with exception to the difference between the high and low workload task. Many of these tasks have been used in previous task-oriented research [24–28]. Multiple modalities were utilized for data collection. The Advanced Brain Monitoring B-Alert X24 was used to collect electroencephalogram data at a frequency of 256 Hz. The MindMedia NeXus-10 system was used to collect electrocardiogram and respiration data at 256 Hz. All measured time series were recorded using MAPPS (EyesDx, Inc., Coralville, IA), a software suite designed to collect aircraft and simulator state, event markers, video, and pilot physiological and behavioral data. The software time synchronizes all data channels for real-time review.

B. Developing HMMs for Cognitive State Detection:

The proposed HMM method is partitioned into four key modeling processes: 1) feature engineering and preprocessing; 2) feature selection; 3) HMM learning and design; and 4) model fusion via HMM stacking. (This stacking concept is commonly used for modeling EEG data with HMMs [29–32].)

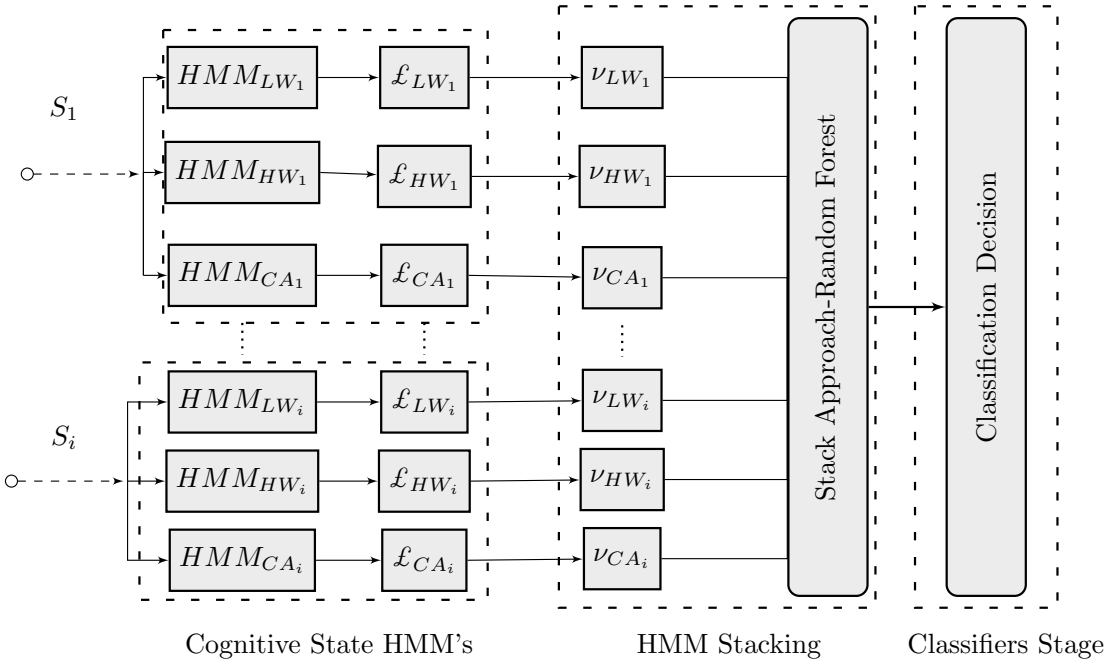

Fig. 1 Stacked HMM Classifier.

1. Feature Engineering and Preprocessing:

The three modalities examined for this study were ECG, Respiration and EEG data, where the first 90 seconds of the data was removed from the benchmark tasks. This was to ensure that the subject was fully within their intended induced cognitive state (i.e., CA, HW, or LW). The ECG data were pre-processed with a bandpass butterworth filter (described in [15]) and the heart rate variability (HRV) was calculated (described in [4]). The ECG data heart rate complexity was calculated using a 90 second moving window, in which the HRV was extracted and sample entropy was calculated for the windowed segment. The EEG data were processed into their respective frequency bands, rank order complexity (ROC) and the engagement index was also calculated (described in [33–35]). Additionally, the respiration complexity, a novel way to examine respiration dynamics and sudden changes in breathing patterns, was also utilized (described in [35]). The data was then normalized per subject per day.

2. Feature Selection:

The applied feature engineering methods produced 285 observed time-series features for each subject's data and cognitive benchmark task. Selecting which features of the observation are relevant and should be used for modeling the data using an HMM can be a difficult problem [36]. One method is to utilize domain knowledge and select features based on the practitioners' intuition about the process being modeled. Another method uses the concept of feature saliency [37, 38]. Feature saliency is essentially a weight between a state-dependent emission distribution and a state-independent emission distribution. Features with a high saliency are more effectively modeled by the state-dependent distribution, and thus assumed to be relevant features for modeling an HMM. The emission distribution for the feature saliency HMM (FSHMM) is written as

$$f_{x_t}(y_t) = \prod_{l=1}^{L} \rho_l r(y_{lt}|\mu_{x_t,l}, \sigma_{x_t,l}) + (1-\rho_l) q(y_{lt}|\epsilon_l, \tau_l), \tag{1}$$

where L is the number of features in the observation vector, x_t represents the state at time t, y_{lt} represents observation of the l^{th} features at t, ρ_l is the feature saliency for the l^{th} feature, $r(\cdot|\cdot)$ is the state-dependent Gaussian emission distribution with mean μ and standard deviation σ, and $q(\cdot|\cdot)$ is the state-independent Gaussian emission distribution with mean ϵ and standard deviation τ. In this study, a combination of domain knowledge and feature saliency was used to select features for the HMMs.

3. HMM Framework and Training:

Once a specific set of features is chosen, an HMM can be trained using the selected features as the observed data. HMMs have been widely used to model time-series data and are composed of two sequences of random variables. The state sequence, represented by X, is assumed to be a latent or unobserved variable and modeled as a Markov chain. The emission sequence, represented by Y, are observed and assumed to be correlated with the state sequence. The components of an HMM are the initial state distribution for the Markov chain π, the transition probabilities of the Markov chain which are often combined into a transition matrix, A, and the parameters of emission distribution. When the emission probabilities are modeled as a Gaussian distribution, these parameters are the mean and standard deviation of the state-conditional distribution. There are three core problems that could be solved when modeling data using HMMs. The first is estimating the probability that the observed sequence, Y, was generated by a specific HMM. This problem can be solved by computing the forward probabilities. The second is estimating an optimal state sequence given Y and an HMM. This problem can be solved using the Viterbi algorithm [39]. The third is estimating the parameters of an HMM given Y. There are numerous solutions to this problem but the most common is to use the expectation-maximization (EM) algorithm.

The HMM stage uses the time series features S as the observations of an HMM. S can be any group of features in the larger feature set, but we generally subset the features by sensor and denote the features from sensor i as S_i. For each feature subset, there are three associated HMMs, one for each class {LW, HW, CA}. The HMMs are trained on data associated with each class (HMM problem 3). The training algorithm is the maximum a posteriori (MAP) formulation of the Baum Welch algorithm [40]. The likelihood of the observation sequence $\mathcal{L} = P(Y|\lambda)$ using the forward probabilities of the forward backward algorithm [19, 20], where λ represents the parameters of the HMM (HMM problem 1). The likelihood that the observation sequence was generated by each HMM is combined in a sub-feature vector and passed to the second stage of the method

$$v = [\mathcal{L}_{LW}\ \mathcal{L}_{HW}\ \mathcal{L}_{CA}]. \tag{2}$$

The sub-feature vector can be combined with other sub-feature vectors from other feature subsets to form V, e.g. $V = [v_{ECG}\ v_{FP1}]$.

4. Stacking HMM Classifiers

The classifier stage uses the sub-features v calculated in the HMM stage as inputs into a classifier. Let i represent the number of sub-feature vectors, then $V = [v_1\ v_2\ \ldots\ v_i]$. As previously mentioned, any type of classifier could be used in this stage, but the proposed implementation uses the random forest algorithm [41]. Figure 1 displays the workflow for the stacked HMM classifier.

C. Complexity Analysis of Psychophysiological Temporal Dynamics of the Hidden Layer

Once the HMM's are trained for the three proposed cognitive states, the underlying state sequence is estimated (HMM problem 2) characterizing the psychophysiological dynamics. In order to analyze an arbitrary discrete integer sequence, we apply permutation entropy, which analyzes how the permutations of the rank order changes to quantify the complexity of time series [42, 43]. We deploy *Permutation Entropy*, by,

$$H_n = -\sum_{j=1}^{n!} p'_j \log_2 p'_j, \tag{3}$$

where p'_j is the proportion of the occurrence of th j^{th} template (of length m) in the signal [42, 43]. A template length of $M = 3$ and $M = 4$, was utilized to explore the complexity changes of the discretized sequence.

III. Results

This section outlines the numerical experiments performed on the data which addresses the following research questions:

1) What features are useful for producing FSHMMs with the distinct pyscho-physiological sub-states?
2) How do different modalities and combinations of modalities affect the classification performance of the cognitive states?

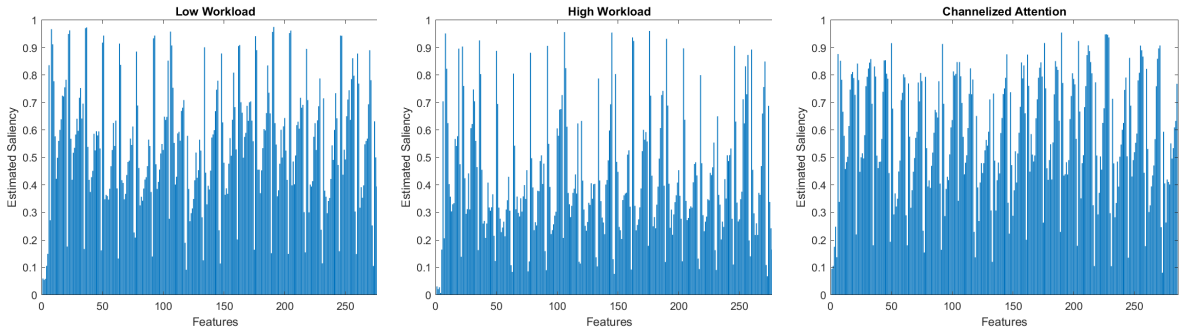

(a) Estimated ρ for LW. **(b) Estimated ρ for HW.** **(c) Estimated ρ for CA.**

Fig. 2 Estimated feature saliencies for each cognitive state. There is a pattern across all cognitive states. The respiration and ECG features have low saliency. The engagement index and ROC for each EEG lead also have low saliency. The first filter for each lead generally has high saliency. The saliency for each successive filter decreases and then begins to rise towards the higher filters. Generally, HW has lower saliency values than the other cognitive states.

3) Does the temporal complexity of the underlying pyschophysiological dynamics of the HMM alter or vary across the three cognitive states (i.e., HW, LW, and CA)?

A. RQ1: Feature Saliency

The MAP formulation of the FSHMM is used to estimate feature saliencies for each feature. The data is not divided into testing and training sets for this analysis. First, for each class a single FSHMM with five states is trained using all 285 possible features. The FSHMM is initialized with even probabilities for the initial state distribution and the transition matrix. The means of the state-dependent emission distributions are initialized using the K-means algorithm, and the standard deviation is initialized by dividing the standard deviation of the data by the number of states. The feature saliencies are initialized as 0.5, and the parameters of the state-independent emission distribution are initialized as the mean and standard deviation of the data. For the hyperparameters, $\beta = \alpha = 2$, $m = \mu_{init}$, $\zeta = \sigma_{init}$, $b = \epsilon_{init}$, $\nu = \tau_{init}$, $s = \eta = c = \psi = 1$, and $k = 100$. Due to the randomness in the K-means algorithm, the training of the FSHMM is repeated ten times with different initial means for the state-dependent distribution.

Figure 2 displays the estimated feature saliencies for each class and the average across the classes. The order of the features is the respiration features, the ECG features, and then the features for each lead of the EEG with engagement index first, ROC second, and then filters 1 through 12. The order of the leads is as listed in Figure 3.

In general, the respiration and ECG features have low saliency. For the EEG features, ROC and engage index also have low saliency. The first filter and the last filter generally have higher saliency than the middle filters. Figure 3 provides details for the estimated saliencies for the EEG filter features. When looking across the cognitive states, high workload generally has lower saliency across all features. This means that the features for high workload have features that are more likely to fit the state-independent distribution than the state-dependent distribution. This could be interpreted as having less activity in the emissions as the state changes or that the emissions tend to change less as the state changes.

When individual FSHMMs are trained using only the respiration features and the ECG features separately, the estimated features saliencies are all above 0.7. We hypothesize that the state sequence in the full model is dominated by the features associated with the EGG leads and therefore minimizes the change in the feature distributions for the ECG and respiration features with respect to the state.

B. RQ2: Classification Performance

A leave-one-out cross validation (LOOCV) testing framework was used to evaluate the classification model proposed in Section II.B. An observation is considered to be the time series for the selected feature subset for each participant on each day. Using this scheme, there are 63 observation sequences. Each LOOCV experiment is run 10 times in order to characterize the variability in classification accuracy due to the random initialization of the HMMs. The HMMs are

	Filter													
EEG Lead	f1	f2	f3	f4	f5	f6	f7	f8	f9	f10	f11	f12	Average	Std
FP1	0.86	0.67	0.50	0.42	0.37	0.40	0.37	0.51	0.56	0.70	0.71	0.71	0.56	0.16
F7	0.88	0.71	0.46	0.41	0.37	0.41	0.45	0.61	0.60	0.70	0.68	0.68	0.58	0.16
F8	0.89	0.72	0.38	0.34	0.36	0.35	0.40	0.57	0.55	0.59	0.55	0.54	0.52	0.17
T4	0.89	0.70	0.32	0.34	0.31	0.36	0.36	0.42	0.49	0.54	0.54	0.52	0.48	0.17
T6	0.82	0.54	0.35	0.40	0.36	0.39	0.41	0.48	0.48	0.53	0.52	0.61	0.49	0.13
T5	0.86	0.48	0.39	0.35	0.30	0.34	0.40	0.46	0.45	0.48	0.57	0.59	0.47	0.15
T3	0.90	0.66	0.36	0.32	0.31	0.35	0.43	0.48	0.53	0.63	0.62	0.64	0.52	0.18
FP2	0.87	0.68	0.55	0.40	0.35	0.34	0.38	0.50	0.54	0.63	0.57	0.70	0.54	0.16
O1	0.67	0.37	0.28	0.31	0.29	0.38	0.38	0.44	0.39	0.44	0.55	0.57	0.42	0.12
P3	0.79	0.37	0.38	0.38	0.31	0.35	0.45	0.53	0.58	0.70	0.70	0.79	0.53	0.18
Pz	0.73	0.45	0.35	0.36	0.37	0.37	0.37	0.47	0.49	0.62	0.66	0.65	0.49	0.14
F3	0.87	0.79	0.48	0.54	0.47	0.51	0.49	0.54	0.54	0.63	0.65	0.68	0.60	0.13
Fz	0.90	0.63	0.44	0.45	0.41	0.40	0.35	0.49	0.56	0.66	0.73	0.70	0.56	0.17
F4	0.91	0.68	0.49	0.45	0.40	0.36	0.40	0.48	0.49	0.60	0.60	0.55	0.53	0.15
C4	0.89	0.67	0.42	0.40	0.39	0.47	0.52	0.58	0.60	0.67	0.61	0.61	0.57	0.14
P4	0.82	0.47	0.30	0.32	0.32	0.43	0.47	0.59	0.57	0.68	0.66	0.77	0.53	0.18
Pz	0.74	0.41	0.31	0.27	0.32	0.33	0.36	0.39	0.46	0.59	0.61	0.64	0.45	0.16
C3	0.89	0.65	0.47	0.50	0.41	0.52	0.58	0.67	0.61	0.73	0.75	0.74	0.63	0.14
Cz	0.88	0.49	0.35	0.33	0.28	0.36	0.38	0.47	0.56	0.69	0.75	0.75	0.52	0.20
O2	0.67	0.37	0.29	0.30	0.38	0.39	0.38	0.41	0.35	0.52	0.55	0.58	0.43	0.12
Average	0.84	0.58	0.39	0.38	0.35	0.39	0.42	0.50	0.52	0.62	0.63	0.65		
Std	0.07	0.14	0.08	0.07	0.05	0.05	0.06	0.07	0.07	0.08	0.07	0.08		

Fig. 3 Table of Estimated Feature Saliencies for EGG filter features.

initialized and have the same hyperparameters as in the previous section but exclude the state-independent distributions and the feature saliencies. The number of states for the HMMs was varied 3 to 8. The random forest algorithm grew 100 trees.

The four sensor groups (SGs) are listed in Table 4. For each sensor group containing an EEG lead, five feature subsets are evaluated. Filter 1 was selected based on the feature saliency analysis. The other feature subsets were selected based on domain knowledge. Table 4 contains the mean classification accuracy for the outlined evaluation. The highest accuracy for this numerical experiments was 50%, which was achieved by several models of different modalities. This occurred three times when the number of states in the HMM was 5, specifically for SG1, SG3, and SG4. This would indicate that adding modalities does not necessarily increase the classification accuracy. To further investigate the predictive ability of these models, Figure 6 displays the confusion matrices for these models. The predictive ability per cognitive state is relatively stable across the sensor groups. All of the models have significant difficulty in classifying the high workload cognitive state. Furthermore, low workload is often confused with channelized attention.

		States					
Sensor Group	Features	3	4	5	6	7	8
SG1: ECG, Respiration, FP1, FP2	Full	0.37	0.39	0.40	0.43	0.39	0.42
	Engage Index	0.40	0.44	0.47	0.47	0.45	0.48
	f1	0.44	0.40	0.50	0.47	0.45	0.49
	ROC	0.36	0.43	0.44	0.43	0.40	0.43
	ROC*f1	0.34	0.37	0.34	0.37	0.37	0.35
SG2: ECG, Respiration, FP1	Full	0.37	0.45	0.46	0.44	0.43	0.42
	Engage Index	0.37	0.40	0.46	0.43	0.41	0.44
	f1	0.44	0.38	0.47	0.43	0.40	0.44
	ROC	0.43	0.50	0.46	0.40	0.35	0.42
	ROC*f1	0.34	0.37	0.36	0.33	0.34	0.38
SG3: ECG, Respiration, FP2	Full	0.40	0.37	0.43	0.41	0.36	0.40
	Engage Index	0.44	0.45	0.49	0.49	0.44	0.46
	f1	0.44	0.40	0.50	0.47	0.45	0.48
	ROC	0.42	0.39	0.49	0.44	0.46	0.50
	ROC*f1	0.33	0.39	0.41	0.40	0.35	0.41
SG4: ECG and Respiration		0.40	0.41	0.50	0.44	0.38	0.40

Fig. 4 Mean Classification Accuracy for Evaluation Experiments.

C. RQ3: Temporal Complexity of a Underlying Psychophysiological Sequence

The permutation entropy that was applied to the hidden layer of the HMM's sequence demonstrates a clear and distinct pattern within and across the EEG and Heart Dynamics modalities.A non-parametric one-way ANOVA, the

		Predicted Class		
		LW	HW	CA
True Class	LW	10	2	12
	HW	4	1	5
	CA	6	2	21

(a) Confusion matrix for SG1.

		Predicted Class		
		LW	HW	CA
True Class	LW	9	1	14
	HW	2	1	7
	CA	7	2	20

(b) Confusion matrix for SG3.

		Predicted Class		
		LW	HW	CA
True Class	LW	12	1	11
	HW	2	1	7
	CA	8	2	19

(c) Confusion matrix for SG4.

Fig. 5 Confusion matrices for different sensor groups.

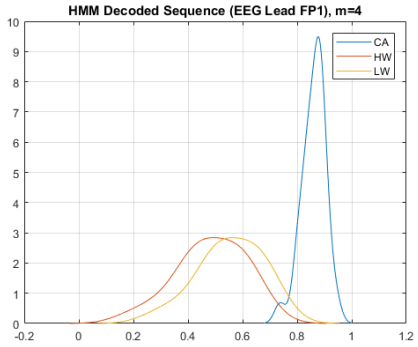

(a) EEG Lead FP1

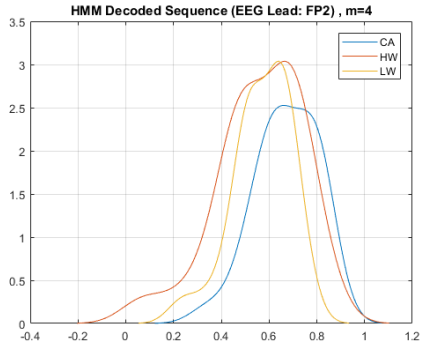

(b) EEG Lead FP2

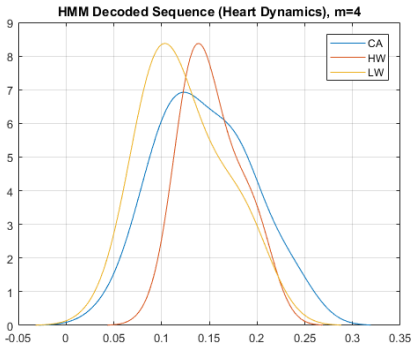

(c) Heart Complexity

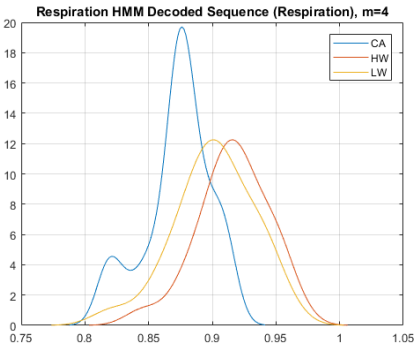

(d) Respiration Complexity.

Fig. 6 This depicts the "Temporal Finger Print" distribution of the proposed cognitive states across various psycho-physiological features. The distribution was formed using a kernel density estimate from the permutation entropy analysis to evaluate the complexity of the decoded hidden layer of the HMM Model.

Kruskal-Wallis test by ranks was applied for the statistical analysis. This statistical significance was consistent for both template lengths of $m = 3$ and $m = 4$, and the template lengths did not alter results of the post-hoc analysis. Thus, the results (e.g., p-values, means, standard deviations) provided are for the higher template length case, m=4. With respect to the underlying psychophysiological dynamics of the HMM statistically differing between the proposed cognitive state, 3 of 4 modalities examined EEG Lead FP1, EEG Lead FP2, and respiration demonstrated statistical significance, where Heart Complexity was not significant but the trends aligned with the EEG modalities. These trends across these modalities demonstrated CA having higher complexity within the hidden layers of the HMM's. More specifically, EEG Lead FP1's CA ($\mu = 0.913$, $\sigma = 0.035$) is significantly higher ($p = 8.53x10^{-11}$), than both LW ($\mu = 0.612$, $\sigma = 0.115$) and HW ($\mu = 0.654$, $\sigma = 0.196$) cognitive states, but HW is not significantly higher than LW. EEG Lead FP2's CA ($\mu = 0.674$, $\sigma = 0.125$) is significantly higher ($p = 1.72x10^{-2}$) than both LW ($\mu = 0.571$, $\sigma = 0.120$) and HW ($\mu = 0.614$, $\sigma = 0.219$) cognitive states, and HW is not significantly higher than LW. On the other hand, respiration complexity, demonstrates a high entropy values relative to the other modalities. Furthermore, within respiration complexity, CA ($\mu = 0.917$, $\sigma = 0.024$) has a significantly lower complexity ($p = 6.93x10^{-4}$) than LW ($\mu = 0.901$, $\sigma = 0.031$) and HW ($\mu = 0.905$, $\sigma = 0.029$).

Across modalities and cognitive states these distributions of the underlying complexity of psychophysiological sequence have multiple modes or are skewed. We may be able to interpret these single mode distributions as an indication that the individual is psychophysiologically locked into the task designed to induce channelize attention. Likewise, non-normal changes within the distribution may provide an indication that the individual is psychophysiologically not engaged into the task designed to induce a cognitive state. Thus, these underlying psychophysiological sequences of discriminating features transitions become less complex for specific individuals on baseline runs. This raises fundamental cognitive questions, if the bi-modal or skewed distribution is related to the subject's complexity dropping because they "gave-up" on the task or became distracted for the high workload and low workload tasks, respectively.

Decision Analysis Point of View: Another approach to evaluate the entropy distributions of the states, beyond visual inspections and ANOVA to verify their statistical differences, is to employ stochastic dominance. Consider that CA, HW, and LW entropy measures have the cumulative distribution functions $F_{CA}(x)$, $F_{HW}(x)$, and $FLW(x)$, where it is desirable to maximize (or easily changed to minimization) the value of entropy "x" (Figure 7 below, for EEG Lead FP1 and with a template length of $m = 4$). It is clear, as was by visual inspection, that the CA entropy has the highest mean and the ANOVA analysis verified that the CA entropy is statistically significantly higher than HW and LW. If, however:

$$F_{HW}(x) \leq F_{CA}(x) \quad \text{and} \quad F_{LW}(x) \leq F_{CA}(x) \quad \text{for all x} \tag{4}$$

then CA stochastically (first order) dominates options HW and LW when considering entropy. This amounts to saying that the CDF of option CA is to the right of that of option HW and LW in the CDF plots in Figure 7:

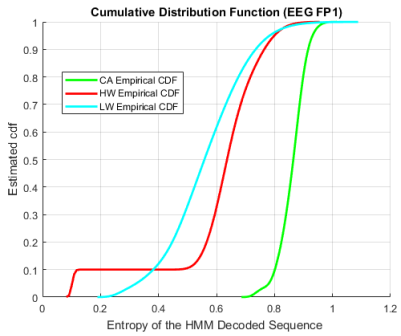

Fig. 7 CDF demonstrating first order stochastic dominates for EEG Lead FP1.

This means that, for the feature FP1 the CA entropy is superior to HW and LW since for any cumulative probability value, it gives a higher entropy (i.e., not just the mean is higher, but the first quartile and the third quartile are also higher). First order stochastic dominance is reasonably intuitive and makes virtually no assumptions about the decision-makers utility function for entropy, only that it is continuous and monotonically increasing with increasing entropy. Such an approach could be considered for all features and metrics. Results such as the figure above, for example, would inform the decision maker that regardless of the utility function we place on the metric entropy, the CA state has highest expected utility.

IV. Conclusion and Future Work

This study has uncovered a deeper understanding of the underlying physiological dynamics that occur over time for specific cognitive states, which we refer to as "physiological temporal fingerprints". We demonstrate that these fingerprints were unique for specific cognitive states through examining the entropy or complexity of how a human's psychophysiological features dynamically change over time. This particular work can potentially advance how we examine cognitive state transitions, the level of cognitive induction from the task, and how we predict cognitive states within the areas of human-machine interaction and human-autonomy teaming.

Future work will seek to incorporate an enhanced interpretation of the cognitive meaning of qualifying this entropy dynamics that related to psychophysiological features (e.g., Degree of "Locked" in to a channelized attention task). Moreover, the predictive accuracy of these work doesn't out preform our past methods [14]. However, the results in this study was evaluated on a limited feature sets when compared to the previous study and improved multi-modal HMM need to continue to be evaluated.

References

[1] Commercial Aviation Safety Team, "SE211: Airplane State Awareness - Training for Attention Management (R-D)," , Mar. 2015. URL http://www.skybrary.aero/index.php/SE211:_Airplane_State_Awareness_-_Training_for_Attention_Management_(R-D).

[2] Commercial Aviation Safety Team, "Airplane State Awareness Joint Safety Analysis Team Interim Report," , Mar. 2015. URL http://www.skybrary.aero/index.php/Commercial_Aviation_Safety_Team_(CAST)_Reports.

[3] Kulic, D., and Croft, E., "Estimating robot induced affective state using hidden markov models," *ROMAN 2006-The 15th IEEE International Symposium on Robot and Human Interactive Communication*, IEEE, 2006, pp. 257–262.

[4] Napoli, N. J., Demas, M. W., Mendu, S., Stephens, C. L., Kennedy, K. D., Harrivel, A. R., Bailey, R. E., and Barnes, L. E., "Uncertainty in heart rate complexity metrics caused by R-peak perturbations," *Computers in biology and medicine*, Vol. 103, 2018, p. 198—207. doi:10.1016/j.compbiomed.2018.10.009.

[5] Fairclough, S. H., Gilleade, K., Ewing, K. C., and Roberts, J., "Capturing user engagement via psychophysiology: measures and mechanisms for biocybernetic adaptation," *International Journal of Autonomous and Adaptive Communications Systems*, Vol. 6, No. 1, 2013, pp. 63–79.

[6] Thomas, L. C., Gast, C., Grube, R., and Craig, K., "Fatigue detection in commercial flight operations: Results using physiological measures," *Procedia Manufacturing*, Vol. 3, 2015, pp. 2357–2364.

[7] Verma, G. K., and Tiwary, U. S., "Multimodal fusion framework: A multiresolution approach for emotion classification and recognition from physiological signals," *NeuroImage*, Vol. 102, 2014, pp. 162–172.

[8] Wilhelm, F. H., and Grossman, P., "Emotions beyond the laboratory: Theoretical fundaments, study design, and analytic strategies for advanced ambulatory assessment," *Biological psychology*, Vol. 84, No. 3, 2010, pp. 552–569.

[9] Wilson, G. F., and Russell, C. A., "Real-time assessment of mental workload using psychophysiological measures and artificial neural networks," *Human factors*, Vol. 45, No. 4, 2003, pp. 635–644.

[10] Brouwer, A.-M., Hogervorst, M. A., Van Erp, J. B., Heffelaar, T., Zimmerman, P. H., and Oostenveld, R., "Estimating workload using EEG spectral power and ERPs in the n-back task," *Journal of neural engineering*, Vol. 9, No. 4, 2012, p. 045008.

[11] Berka, C., Levendowski, D. J., Lumicao, M. N., Yau, A., Davis, G., Zivkovic, V. T., Olmstead, R. E., Tremoulet, P. D., and Craven, P. L., "EEG correlates of task engagement and mental workload in vigilance, learning, and memory tasks," *Aviation, space, and environmental medicine*, Vol. 78, No. 5, 2007, pp. B231–B244.

[12] Palinko, O., Kun, A. L., Shyrokov, A., and Heeman, P., "Estimating cognitive load using remote eye tracking in a driving simulator," *Proceedings of the 2010 symposium on eye-tracking research & applications*, ACM, 2010, pp. 141–144.

[13] Marshall, S. P., "Identifying cognitive state from eye metrics," *Aviation, space, and environmental medicine*, Vol. 78, No. 5, 2007, pp. B165–B175.

[14] Harrivel, A. R., Stephens, C. L., Milletich, R. J., Heinich, C. M., Last, M. C., Napoli, N. J., Abraham, N., Prinzel, L. J., Motter, M. A., and Pope, A. T., "Prediction of cognitive states during flight simulation using multimodal psychophysiological sensing," *AIAA Information Systems-AIAA Infotech@ Aerospace*, 2017, p. 1135.

[15] Napoli, N., and Barnes, L., "A Dempster-Shafer Approach for Corrupted Electrocardiograms Signals," *AAAI Publications, The 29th International Flairs Conference*, 2016.

[16] Simola, J., Salojärvi, J., and Kojo, I., "Using hidden Markov model to uncover processing states from eye movements in information search tasks," *Cognitive systems research*, Vol. 9, No. 4, 2008, pp. 237–251.

[17] Liechty, J., Pieters, R., and Wedel, M., "Global and local covert visual attention: Evidence from a Bayesian hidden Markov model," *Psychometrika*, Vol. 68, No. 4, 2003, pp. 519–541.

[18] Haapalainen, E., Kim, S., Forlizzi, J. F., and Dey, A. K., "Psycho-physiological measures for assessing cognitive load," *Proceedings of the 12th ACM international conference on Ubiquitous computing*, ACM, 2010, pp. 301–310.

[19] Rabiner, L. R., "A tutorial on hidden Markov models and selected applications in speech recognition," *Proceedings of the IEEE*, Vol. 77, No. 2, 1989, pp. 257–286.

[20] Juang, B. H., and Rabiner, L. R., "Hidden Markov models for speech recognition," *Technometrics*, Vol. 33, No. 3, 1991, pp. 251–272.

[21] Yoon, B.-J., "Hidden Markov models and their applications in biological sequence analysis," *Current genomics*, Vol. 10, No. 6, 2009, pp. 402–415.

[22] Duda, R. O., Hart, P. E., and Stork, D. G., *Pattern classification*, John Wiley & Sons, 2012.

[23] Harrivel, A. R., Liles, C., Stephens, C. L., Ellis, K. K., Prinzel, L. J., and Pope, A. T., "Psychophysiological sensing and state classification for attention management in commercial aviation," *AIAA Infotech@ Aerospace*, 2016, p. 1490.

[24] Fairclough, S., and Gilleade, K., "Construction of the biocybernetic loop: a case study," *Proceedings of the 14th ACM international conference on Multimodal interaction*, ACM, 2012, pp. 571–578.

[25] Gross, J. J., and Levenson, R. W., "Emotion elicitation using films," *Cognition & emotion*, Vol. 9, No. 1, 1995, pp. 87–108.

[26] Parasuraman, R., and Davies, D., "A taxonomic analysis of vigilance performance," *Vigilance*, Springer, 1977, pp. 559–574.

[27] Santiago-Espada, Y., Myer, R. R., Latorella, K. A., and Comstock Jr, J. R., "The multi-attribute task battery ii (matb-ii) software for human performance and workload research: A user's guide," 2011.

[28] Stephens, C. L., Christie, I. C., and Friedman, B. H., "Autonomic specificity of basic emotions: Evidence from pattern classification and cluster analysis," *Biological psychology*, Vol. 84, No. 3, 2010, pp. 463–473.

[29] Lee, H., and Choi, S., "PCA+ HMM+ SVM for EEG pattern classification," *Seventh International Symposium on Signal Processing and Its Applications, 2003. Proceedings.*, Vol. 1, IEEE, 2003, pp. 541–544.

[30] Li, Y., Dong, G., Gao, X., Gao, S., Ge, M., and Yan, W., "Single trial EEG classification during finger movement task by using hidden Markov models," *Conference Proceedings. 2nd International IEEE EMBS Conference on Neural Engineering, 2005.*, IEEE, 2005, pp. 625–628.

[31] Suk, H.-I., and Lee, S.-W., "Two-layer hidden Markov models for multi-class motor imagery classification," *2010 First Workshop on Brain Decoding: Pattern Recognition Challenges in Neuroimaging*, IEEE, 2010, pp. 5–8.

[32] Wissel, T., Pfeiffer, T., Frysch, R., Knight, R. T., Chang, E. F., Hinrichs, H., Rieger, J. W., and Rose, G., "Hidden Markov model and support vector machine based decoding of finger movements using electrocorticography," *Journal of neural engineering*, Vol. 10, No. 5, 2013, p. 056020.

[33] Pope, A., Bogart, E., and Bartolome, D., "Biocybernetic system evaluates indices of operator engagement in automated task." *Biological Psychology*, Vol. 40, 1995, pp. 187–195.

[34] Napoli, N. J., Demas, M., Stephens, C. L., Kennedy, K. D., Harrivel, A. E., Barnes, L., and Pope, A. T., "Activation Complexity: A Cognitive Impairment Tool for Characterizing Neuro-isolation." *Nature Scientific Review*, In Review, pp. 311–318.

[35] Napoli, N., *Characterizing Uncertainty in Sensor Fusion to Improve Predictive Models*, Online Archive of University of Virginia, 2018.

[36] Adams, S., and Beling, P. A., "A survey of feature selection methods for Gaussian mixture models and hidden Markov models," *Artificial Intelligence Review*, Vol. 52, No. 3, 2019, pp. 1739–1779.

[37] Adams, S., Beling, P. A., and Cogill, R., "Feature selection for hidden Markov models and hidden semi-Markov models," *IEEE Access*, Vol. 4, 2016, pp. 1642–1657.

[38] Adams, S., and Beling, P. A., "Feature selection for hidden Markov models with discrete features," *Proceedings of SAI Intelligent Systems Conference*, Springer, 2019, pp. 67–82.

[39] Viterbi, A., "Error bounds for convolutional codes and an asymptotically optimum decoding algorithm." *IEEE Transactions on Information Theory*, Vol. 13, 1967, pp. 260—-269.

[40] Gauvain, J.-L., and Lee, C.-H., "Maximum a posteriori estimation for multivariate Gaussian mixture observations of Markov chains," *IEEE transactions on speech and audio processing*, Vol. 2, No. 2, 1994, pp. 291–298.

[41] Breiman, L., "Random forests," *Machine learning*, Vol. 45, No. 1, 2001, pp. 5–32.

[42] Bandt, C., and Pompe, B., "Permutation Entropy: A Natural Complexity Measure for Time Series," *Phys. Review Letters*, Vol. 88, No. 17, 2002.

[43] Riedl, M., Müller, A., and Wessel, N., "Practical considerations of permutation entropy," *The Euro. Phys. Jour. Special Topics*, Vol. 222, No. 2, 2013, pp. 249–262.